Elsevier Editorial System(tm) for
International Journal of Fatigue
Manuscript Draft

Manuscript Number:

Title: Fatigue life estimation of cast aluminum alloys considering the effect of porosity on initiation and propagation phases

Article Type: Original Research Paper

Keywords: cast aluminium alloys; casting defects; porosity; fatigue life

Corresponding Author: Dr. Jon Ander Esnaola, Ph.D

Corresponding Author's Institution: Universtiy of Mondragon

First Author: Raquel Hidalgo

Order of Authors: Raquel Hidalgo; Jon Ander Esnaola, Ph.D; Iñigo Llavori; Miren Larrañaga; Iñaki Hurtado; Nuria Herrero-Dorca

Manuscript Region of Origin: Europe

Raquel Hidalgo & Jon Ander Esnaola
Mondragon Unibertsitatea
+34 606 871 170
+34 635 739 144
rhidalgo@mondragon.edu
jaesnaola@mondragon.edu

Prof. M.N. James

Editor

International Journal of Fatigue

8th Janurary 2018

Dear Prof. James

We are pleased to submit the research article entitled "Fatigue life estimation of cast aluminium alloys considering the effect of porosity on the initiation and propagation phases" by R. Hidalgo, J. A. Esnaola, I. Llavori, M. Larrañaga, I. Hurtado and N. Herrero-Dorca to be considered for publication in the *International Journal of Fatigue*. We declare that this manuscript is original, it has not been published and it is not under consideration for publication elsewhere.

Fatigue phenomena is characterised by a high life scatter related to many factors such as notches, stress concentrators, surface quality or residual stresses. In casting components, this scatter is even more notorious due to the defects generated during the manufacturing process. Among the different type of defects, many authors have reported that porosity is one of the main parameter in fatigue life of casting aluminium alloys as affects in crack initiation and propagation phases. However, most of fatigue life estimation models only consider the effect of the initial pore in the fatigue limit and, therefore, present a lack of precision in life estimation. Therefore, the present work is focused on the development of a new fatigue model to improve life prediction accuracy of casting components by considering the effect of porosity in both, the initiation and propagation phases. The model was implemented for Low Pressure Die Casting (LPDC) A356-T6 aluminium alloy and it was validated against LPDC specimens obtained from automotive knuckles arms.

The main findings of the present work are:

- The proposed model presents high accuracy in the fatigue life prediction of LPDC A356-T6 showing a quantitative logarithmic average error below 2% and an absolute average error below 16 %.
- In addition, it is demonstrated that considering the effect of porosity in both, initiation and propagation phases, it is possible to qualitatively predict the scatter trend of each tested sample at each specific testing load.
- The porosity parameters required by the model are difficult to be measured before the rupture of the tested samples. However, in high series applications, such as automotive industry, where thousands of different components in the same material and facilities are manufactured per year,

the statistic data of the required parameters could be easily obtained by characterising the process window. Then, the proposed model can be used as a high precision predictive tool in the design process of new casting components.

We believe this work is suitable for publication in the International Journal of Fatigue. Please, let us know if we can provide any additional information.

Thank you for your consideration.

Yours sincerely,

M.S. Raquel Hidalgo and Dr. Jon Ander Esnaola

Mondragon Unibertsitatea

Corresponding author:

Jon Ander Esnaola

jaesnaola@mondragon.edu

cell:+34 635 739 144

Fatigue life estimation of cast aluminum alloys considering the effect of porosity on initiation and propagation phases.

R. Hidalgo[a,b], J. A. Esnaola[a], I. Llavori[a], M. Larrañaga[a], I. Hurtado[b], N. Herrero-Dorca[b]

[a] Structural Mechanics and Design, Engineering Faculty, Mondragon Unibertsitatea, Mondragon, Spain

[b] Advanced Material Forming Processes, Engineering Faculty, Mondragon Unibertsitatea, Mondragon, Spain

ABSTRACT

Porosity is one of the main parameters in the fatigue life of cast alloys as it affects in both crack initiation and propagation phases. However, most fatigue assessment models consider only the effect of the initial pore in the fatigue limit. Therefore, current approaches present a lack of precision in life estimation. In addition, they are not able to consider the scatter of different samples tested at the same load. As an alternative, in the present study a fatigue assessment model, which accounts the effect of porosity in the initiation and propagation phases, is proposed for Low Pressure Die Casting (LPDC) A356-T6 aluminium alloy. Results have shown that the proposed model is able to qualitatively predict the scatter trend of samples tested at the same load. In addition, the model presents high quantitative accuracy in life estimation with an average logarithmic error below 2% and absolute average error below 16%.

Keywords: cast aluminium alloys, casting defects, porosity, fatigue life.

NOMENCLATURE

AFD	Average Feret Diameter (mm)
f_p	fractographic average porosity (%)
N_p	cycles corresponding to propagation
K_{max}	maximum stress intensity factor (MPa√mm)
N_b	number of cycles calculated with Basquin equation
S_a	stress amplitude (MPa)
N_i	cycles corresponding to initiation
p_r	propagation speed ratio
$C(N_b)$	correction function
N_t	total predicted fatigue life
N_{exp}	number of cycles corresponding to the failure of the specimen
α	fraction of initiation life out of the total
d_V	vertical distance from the initial pore to the surface (mm)
φ	Feret's diameter of the initial pore (mm)

1 INTRODUCTION

Casting aluminium alloys are widely employed in the automotive industry due to their high strength to weight ratio. Particularly, structural components such as knuckles, suspension components or brake callipers, among others, are subjected to severe cyclical loads and, consequently, they can undergo fatigue problems. Fatigue phenomena is characterised by a high life scatter related to many factors such as notches, stress concentrators, surface quality or residual stresses [1]. In casting components, this scatter is even more notorious due to microstructural inhomogeneities and defects such as porosity or inclusions[2]. Thus, Low Pressure Die Casting

(LPDC) is especially interesting to manufacture this type of components as it provides lower porosity and defects than other casting techniques [3].

Several studies demonstrated that, in presence of defects, the effect of microstructural aspects such as SDAS, grain size or eutectic particles in the fatigue behaviour can be neglected [4,5]. The main defects that affect the fatigue life of casting components are porosity and inclusions. Between them, many authors have reported porosity as the most detrimental parameter [6–8].

A wide amount of studies can be found in the literature focused on the influence of porosity in the fatigue life of casting components. Most of the works analyse the influence of surface or near surface pores in the crack initiation stage and its influence in the total fatigue life [4,8–13]. The pores reduce the time to crack initiation by creating a high-stress concentration region adjacent to this microstructural defect [9]. Thus, many authors have proposed fatigue limit estimation procedures dependent on different parameters of the initial pore. The Linear Elastic Fracture Mechanics (LEFM) approach was one of the most widely used technique [6,14]. Alternative works, as the conducted by Murakami *et al.* [15] estimated the fatigue limit considering the $\sqrt{area}$ parameter related to the defect size. Others works such us the Theory of Critical Distances (TCD) prosed by Susmel and Taylor [16] and the Gradient Criterion (GR) proposed by Nadot [17] considered the stress field around a defect to predict the fatigue life of the studied component. However, all these methods only take into account the effect of the initial pore on the fatigue limit.

In contrast, some authors pointed out that not only the initial pore has an effect on the fatigue behaviour of casting Al alloys but also the overall microporosity present in the samples, which has an effect on propagation phase [7,18–20]. Thus, H. R. Ammar *et al.* [21] demonstrated that the high stress concentration associated with large pores (gas pores) increases the crack propagation rate compared to the effect of small multiple pores (shrinkage porosity) for similar average porosity values, decreasing the fatigue life. In addition, higher microporosity level also increases the crack propagation rate[18].

However, few fatigue life estimation approaches in the literature consider the influence of the microporosity in the crack propagation. Choong Do Lee *et al.* [7] proposed a modification of Baquin's equation including the effect of microporosity in fatigue life prediction. However, the proposed procedure presents still a lack of accuracy.

In conclusion, the different approaches found in the literature have still a lack of precision concerning to fatigue life estimation of cast components as they do not consider the effect of porosity in both initiation and propagation phases. In order to face such limitations, in the present work an alternative fatigue model that considers the effect of porosity in both the initiation and propagation phases is proposed.

2 THEORETICAL PROCEDURE

In most of the fatigue assessment models, the behaviour of the material or the studied component is represented by a curve, which provides a relation between the loading, stress or strain, and the estimated life. However, fatigue specimens or components do not show repetitive behaviour when tested at the same load condition due to many factors such as defects or surface finish and, therefore, a scatter in fatigue life is found. The effect of such factors is generally considered by means of coefficients that transform the load/life curve into a scatter band. Particularly, porosity was reported as the main affecting defect in the fatigue life for casting components [6–8]. As an alternative, the proposed procedure pretends to capture the effect of porosity found in the tested specimens or components in both initiation and propagation phases, to provide individual life estimation and minimize the problem of scattering. The proposed procedure is limited to HCF regime and it was developed for A356-T6 aluminium alloy obtained by LPDC. The procedure consists of the following steps:

1. **Material S-N curve characterisation:** As most of HCF assessment methods, the proposed procedure requires to characterize the S-N curve of the material as a starting point. In addition, fracture surfaces have to be analysed to obtain the fractographic

average porosity (f_p) and the average size of pores represented by the Average Feret Diameter (*AFD*).

2. **Propagation model considering porosity:** Following, a propagation analytic model that considers the effect of f_p and the *AFD* of the evaluated specimen/component in the propagation speed is applied. The variation of the propagation speed with respect to the material data case is directly related to the propagation cycles. Thus, the propagation number of cycles N_p can be estimated. The propagation model was obtained through a numeric crack propagation sensitivity study for a determined f_p and *AFD* range according to typical LPDC components data.
3. **Initiation model considering initial pore:** Once propagation cycles are determined, initiation cycles N_i are estimated according to an analytic model that considers the effect of the initiation pore size and the distance to surface in each evaluated case. The initiation model is based on the maximum stress intensity factor K_{max} and the cycle regime. Thus, the same stress intensity factor has a different effect in the initiation phase if the evaluated case is in the lower or the higher domain of the HCF regime. The maximum stress intensity factor K_{max} is given by an analytic equation obtained through a numeric sensitivity analysis that considers the initial pore size and the distance to the surface. The sensitivity analysis range was set for typical LPDC components data values. The cycle domain inside the HCF regime is provided by Basquin total life N_b according to the initial S-N curve.
4. **Total life estimation:** Once propagation cycles N_p and initiation cycles N_i are estimated, total life estimation can be obtained particularised for each evaluated case.

The procedure was implemented to evaluate the fatigue life of specimens obtained from LPDC components and experimentally validated.

2.1 Propagation model considering porosity

As it was exposed in the introduction, porosity has a negative effect in the crack propagation phase. Thus, higher porosity level implies a higher propagation rate and lower propagation number of cycles to final failure [18]. Moreover, for the same porosity level, propagation rate varies depending on the pore size [11]. For this reason, the present model considers both the effect of porosity f_p and the average pore size *AFD,* in the crack propagation speed.

To obtain the propagation model, firstly, specimens used in the initial S-N curve characterisation where the crack initiation pore was located in the surface were identified. It was assumed that, in those cases, the crack initiation cycles are negligible and total life N_t and propagation life N_p can be considered the same. Thus, those cases were considered as reference cases and the propagation speed ratio for their average f_p and *AFD* values was set to p_r=1.

Then, XFEM crack propagation simulations were performed for a specified f_p and *AFD* range according to typical LPDC components data (f_p range from 0.5-4% and *AFD* range from 0.1-0.3 mm). Thus, the response surface of the propagation speed with respect of the reference cases ratio p_r was obtained. Fig. 1 shows the XFEM 2D plane strain model domain of 14x7 mm^2. Pores were modelled as perfect equidistant circles of diameter equal to the *AFD* value of each simulated case and f_p was related to the number of pores for the defined domain cross-section. A general mesh size of 0.5 mm and local mesh size of 0.03 mm near the pores was employed. The Paris coefficients $C=0.9981$ m/cycle/(MPa·√m)^m and $m=9.11\cdot10^{-8}$ corresponding to an A356-T6 alloy were used [22]. The crack propagation architecture used was the one presented by Llavori in 2016 [23]. As a result, the propagation speed ratio response surface $p_r(f_p,AFD)$ with respect to the reference p_r=1 case was obtained. Table 1 shows the simulated f_p and *AFD* cases.

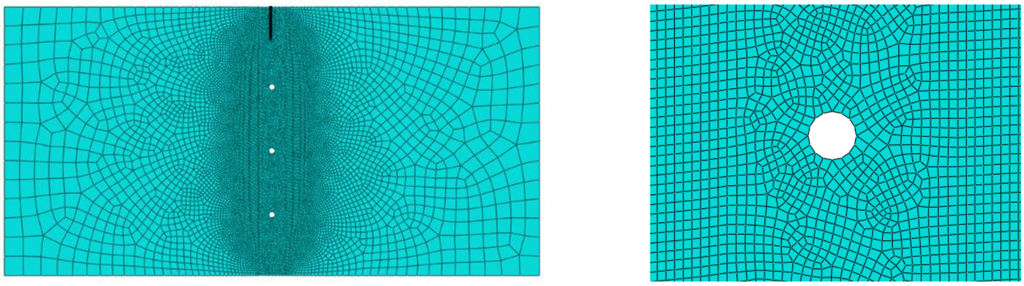

(a) (b)

Fig. 1. a) XFEM propagation model and b) Detail of the local mesh around the pores.

Table 1. f_p and AFD cases considered to obtain the pr(f_p,AFD) surface response

f_p **(%)**	0.5	1.5	3	4	-
AFD	0.1	0.15	0.2	0.25	0.3

Once $p_r(f_p, AFD)$ was obtained, the propagation number of cycles N_p was estimated. For that purpose, a correction function $C(N_b)$ that correlates the Basquin total life prediction N_b (1) with the corresponding N_p was used together with $p_r(f_p, AFD)$ (2).

$$N_b = \left(\frac{S_a}{\sigma'_f}\right)^{\frac{1}{b}} \tag{1}$$

$$N_p\left(f_p, AFD\right) = N_b \frac{C(N_b)}{p_r(f_p, AFD)} \tag{2}$$

The correction function $C(N_b)$ was obtained by applying the best fit technique to the corresponding $C(N_{b\_i})$ values of each reference specimen where the initiation phase was negligible. In addition, each specimen's propagation speed ratio $p_{r\_i}(f_p, AFD)$ was considered. Thus, the total life $N_{exp\_ref\_i}$ of each reference case can be considered equal to the propagation cycles $N_{p\_ref\_i}$ and correlated with each Basquin total life prediction N_{b_i} with the corresponding $C(N_{b\_i})$ value (3), (4).

$$N_{exp\_ref\_i} = N_{p\_ref\_i} = N_{b\_i} \frac{C(N_{b\_i})}{p_{r\_i}(f_p, AFD)} \tag{3}$$

$$C(N_{\mathrm{b}\_i}) = \frac{N_{\mathrm{t\_ref}\_i}\, p_{\mathrm{r}\_i}(f_{\mathrm{p}}, AFD)}{N_{\mathrm{b}\_i}} \tag{4}$$

2.2 Initiation model considering initial pore

Based on Murakami's assumption, the crack initiation phase is related to the maximum stress intensity factor K_{max} generated by near surface pores [15]. Thus, high K_{max} values accelerate crack initiation and consequently reduce the initiation cycles N_{i} to the total life N_{t} ratio [9,21]. In addition, not only K_{max} affects initiation cycles ratio, but also depends on the total cycle range of the evaluated case. For this reason, in the lower cycle domain inside the HCF regime, the N_i to N_{t} ratio is considerably lower than in the higher cycle domain [9]. Consequently, the initiation cycles N_{i} were estimated as a ratio of the total life N_{t} (5) by means of the function $\alpha(K_{\mathrm{max}}, N_b)$ dependent on the stress intensity factor K_{max} and cycle domain represented by the Basquin total life N_b of the evaluated case.

$$N_i = \alpha(K_{\mathrm{max}}, N_{\mathrm{b}})N_{\mathrm{t}} \tag{5}$$

For that purpose, firstly an analytical model to estimate stress intensity factor K_{max} depending on the initial pore characteristics was obtained. Then, the function $\alpha(K_{\mathrm{max}}, N_b)$ that determines the N_{i} cycles to total life N_{t} ratio was established.

2.2.1 Stress intensity factor model depending on the initial pore

To develop the stress intensity factor model, firstly the most relevant initial pore characteristics were identified. According to many authors [15,24], the key factors in the calculation of K_{max} are the distance to the surface d_{V} and the size of the pore φ. Besides these, some authors also reported the morphology of the pores as a relevant factor in the stress intensity factor calculation [25]. Therefore, a two-level numerical sensitivity analysis was performed considering the three main parameters reported in the literature. In addition, horizontal distance to crack tip d_h and pore orientation considering morphology were also included. For the morphology sensitivity analysis, two real initial pores geometries in the fracture surface were selected. The first with a smooth pseudo-spherical shape and the second with an irregular dendritic shape. Table 2 shows the studied pore variables as well as the defined range values. All different pore parameter values were specified from LPDC component fractographic analysis data.

Table 2. Pore variables and ranges considered for the stress intensity factor model.

Factor	Min value	Max value
Vertical distance (d_V)	0.05	0.5
Horizontal distance (d_H)	0	0.1
Feret diameter (φ)	0.1	0.3
Orientation	0º	90º
Morphology	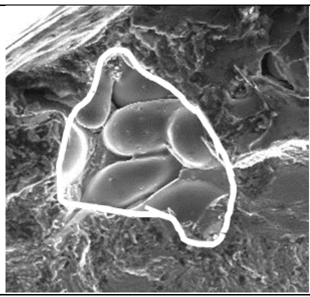	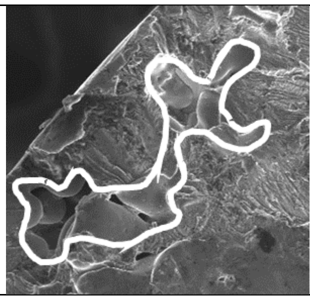

The simplified numeric sensitivity analysis was performed by means of a 5x2.5 mm^2 2D plane strain XFEM model where the real pore geometries, digitalized from the fractographic study were implemented as shown in Fig. 2. A global mesh size of 0.5 mm and local mesh size of 0.005 mm near the pores were used. An initial crack of 0.5 mm length was defined in the centre of the top side of the model and the different pore geometries were located in the vertical and horizontal position as well as in angle with respect it.

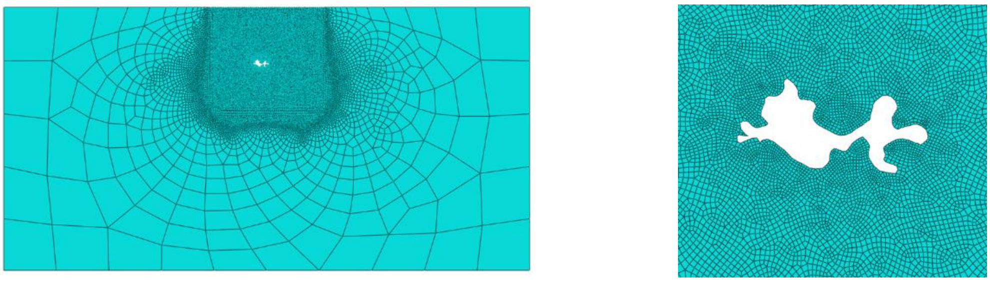

(a) (b)

Fig. 2. a) XFEM model used for the first DOE. b) Zoom of the mesh around the pore.

From the first analysis, the two most influential parameters, the Feret Diameter φ and the vertical distance to surface d_v, were identified. Then, a second analysis was performed in order to obtain the K_{max} response surface equation with respect of both parameters. Table 3 shows the studied conditions within the specified range.

Table 3. Values for dv, and φ used in the second analysis to obtain the K_{max} *response surface equation.*

Factor	Value 1	Value 2	Value 3	Value 4	Value 5	Value 6	Value 7
d_V (mm)	0.01	0.03	0.05	0.1	0.2	0.5	0.7
φ (mm)	0.1	0.3	0.5	1	-	-	-

2.2.2 Initiation cycles to total ratio function

The function $\alpha(K_{max}, N_b)$ that determines the N_i to total life N_t ratio is obtained by means of the following procedure:

1. **Estimation of each specimen's initiation number of cycles:** First, the initiation number of cycles of each tested specimen during the S-N curve characterisation was estimated. For that purpose, propagation cycles of each specimen were estimated based on the N_p estimation procedure presented in section 2.1. Then, initiation cycles of each tested specimen were obtained as the difference between the experimental total life and the estimated propagation number of cycles (6)

$$N_i = N_{exp} - N_p \qquad (6)$$

2. **Obtaining α value for each specimen:** Once the initiation number of cycles of each specimen was estimated, the particular α value for each specimen was obtained (7)

$$\alpha = N_i / N_{exp} \qquad (7)$$

3. **Obtaining K_{max} for each specimen:** Based on the fractographic study data, the K_{max} valued for each specimen was estimated considering the initial pore size φ and the distance to surface d_v based on the procedure presented in section 2.2.1.

4. ***Obtaining the $\alpha(K_{max}, N_b)$* surface equation:** Finally, the α value for each specimen was represented with respect of the estimated K_{max} and N_b values and the $\alpha(K_{max}, N_b)$ surface

equation was obtained by means of best fit technique. For a better performance of the best fit technique two additional constraints were specified:

i. For K_{max} values above 650 MPa√mm, which corresponds to the specimens where the initial pore was located in the surface, the initiation phase was neglected and, consequently $\alpha=0$.

ii. Wang *et al.* [6] reported for an A356-T6 aluminium alloy that a pore with a size less than 25-50 μm did not produce propagation. Consequently, for pore sizes below 25 μm, which corresponds with a K_{max} lower than 385 MPa√mm, the α value was set to 1.

2.3 Total life estimation

Once the propagation number of cycles N_p and $\alpha(K_{max}, N_b)$ of the evaluated case can be estimated considering f_p, AFD, φ and d_v, the total life can be obtained as follows (8, 9, 10):

$$N_t = \alpha \cdot N_t + N_p \quad (8)$$

$$N_t (1-\alpha) = N_p \quad (9)$$

$$N_t = N_p / (1-\alpha) \quad (10)$$

3 EXPERIMENTAL PROCEDURE

3.1 S-N curve characterisation

The S-N curve characterisation of the A356-T6 alloy was conducted with specimens of 6 mm diameter and 40 mm gauge length, according to ASTM-E466 standard, obtained from LPDC automotive knuckle arms. Fig. 3a) and b) show respectively the specimens dimensions and the location in the knuckle arm from where they were obtained.

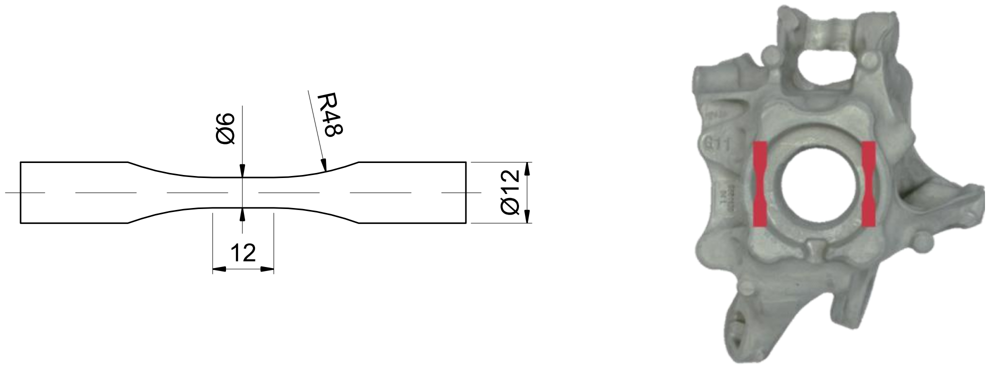

(a) (b)

Fig. 3. a) Fatigue specimens dimensions and b) location in the LPDC knuckle arm from where they were obtained

The fatigue tests were performed using an MTS 810 servo-hydraulic test machine at a stress ratio R=-1 and a frequency of 10 Hz according to ASTM-E466 standard. Four stress amplitudes were tested for characterization: 120, 110, 80 and 70 MPa.

3.2 Fractographic analysis

After tested, a fractographic analysis of all the specimens used in the S-N curve characterisation stage as well as the ones used in the procedure validation stage was performed to obtain the fractographic porosity f_p, Average Feret Diameter *AFD*, the Feret Diameter φ of the pore where the crack initiated and the distance to surface d_v. For that purpose, fracture surface examination was carried out using an FEI Nova Nano SEM 450. The f_p, expressed as the ratio between the area of pores and the entire area of the fracture surface, as well as the *AFD*, initial pore size φ and distance to surface d_v were measured using the software Image J [26].

3.3 Experimental model validation tests

The proposed fatigue model was developed based on the S-N curve characterisation specimens' data. In order to validate the accuracy of the proposed model, additional fatigue tests were performed following the same methodology explained in section 3.1. Specimens were also obtained from LPDC knuckle arms at same locations. Validation tests were performed at *R*=-1 stress amplitudes of 110, 100, 85, and 75 MPa.

4 RESULTS AND DISCUSSION

4.1 Characterisation of LPDC A356-T6

4.1.1 S-N curve characterization

Fig. 4 shows the life of the specimens tested at the specified load levels as well as the fitted Basquin S–N curve (dotted line) with the following parameters: $\sigma_f{}'$ =1191.79 MPa and *b*= -0.1981. It can be observed that the scatter in life for the same load level increases for the higher domain in the HCF regime.

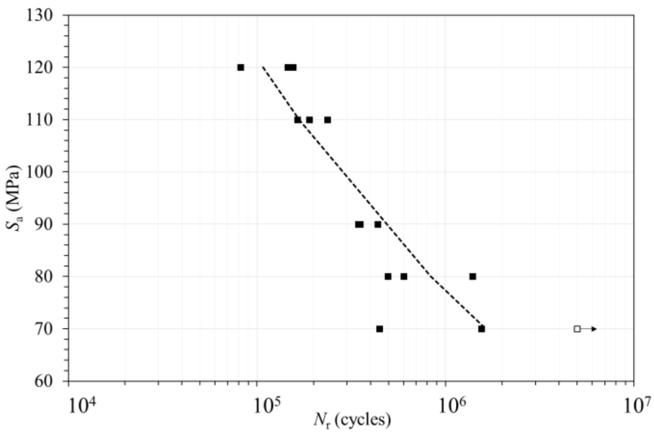

Fig. 4. S-N characterization curve.

4.1.2 Fractographic analysis

Fig. 5. shows an example of a specimen fracture surface a) where the pores along the surface and b) the crack initiation pore are highlighted.

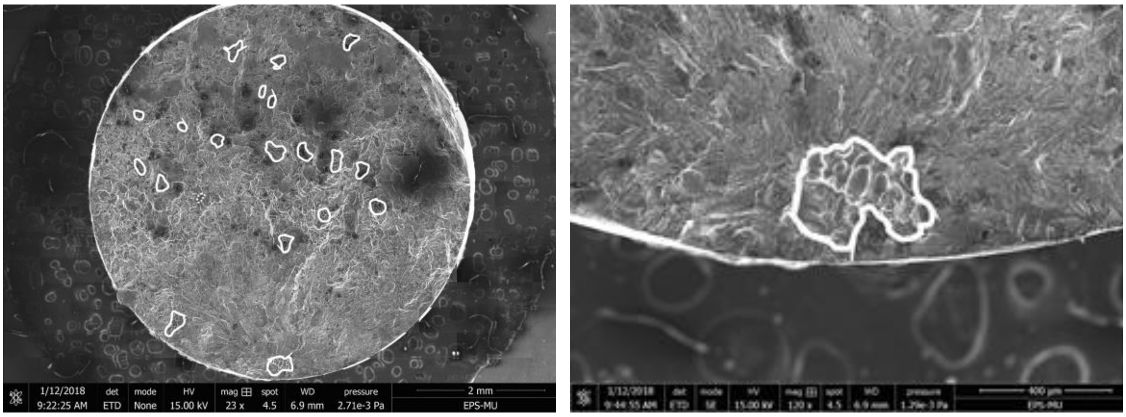

(a) (b)

Fig. 5. Examples of a) fracture surface with f$_p$ *highlighted b) initial pore.*

The results of the fractographic inspection of the specimens used for the S-N curve characterisation are set out in Table 4. As it can be observed, for each stress amplitude the fatigue life decreases with increasing f_p and φ.

Table 4. Results of porosity for the samples used in characterization.

Id.	S_a **(MPa)**	N_{exp} **(cycles)**	**Fractographic porosity**		**Initial pore**	
			f_p**%**	***AFD* (mm)**	***φ* (mm)**	d_V **(mm)**
C_120_1	120	155765	0.66	0.12	0.146	0
C_120_2	120	145470	1.7	0.16	0.344	0
C_120_3	120	81898	3.18	0.2	0.547	0
C_110_1	110	189654	0.95	0.12	0.249	0.015
C_110_2	110	164285	4.34	0.25	0.570	0
C_110_3	110	236106	0.51	0.13	0.127	0.012
C_90_1	90	344584	0.96	0.15	408.9	0
C_90_2	90	352414	2.92	0.15	440	0.040
C_90_3	90	437269	0.76	0.11	192.9	0.044
C_80_1	80	599318	1.23	0.10	0.193	0
C_80_2	80	1393739	0.64	0.14	0.148	0
C_80_3	80	495164	0.88	0.15	0.260	0
C_70_1	70	1550358	1.34	0.16	0.214	0
C_70_2	70	447473	3.29	0.24	0.86	0
C_70_3	70	Run Out	-	-	-	-

4.2 Propagation model

To obtain the propagation model, first reference specimens where the crack initiation pore was located in the surface, and consequently initiation cycles are negligible, were identified. Thus, the reference propagation speed ratio p_r=1 was stablished for the average measured values of f_p=2.56 and *AFD*=0.20 mm. Fig. 6 a), b) and c) shows respectively fractographic analysis examples of crack initiation pores (highlighted in red) located in the surface of specimens tested at stress amplitudes of 120, 90 and 70 MPa.

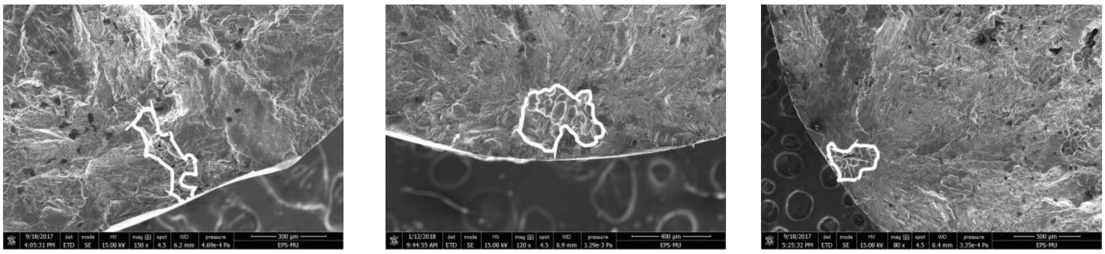

a) S_a=120MPa b) S_a=90MPa c) S_a 70MPa

Fig. 6. Examples of crack initiation pores located in the surface of specimens tested at a)120MPa, b) 90MPa and c) 70MPa stress amplitudes

Following, the propagation speed ratio surface response $p_r(f_p,AFD)$ (11) within the specified f_p and *AFD* range was obtained from the XFEM sensitivity study (Fig. 7). It is observed that, as pointed out in the literature [11,18], the increase of both f_p and *AFD*, increase the propagation rate. However, it can be highlighted that, for the studied range, f_p is the mainly affecting parameter while *AFD* presents a lower effect. The obtained $p_r(f_p,AFD)$ equation (11) allows to estimate the propagation speed ratio within the specified LPDC range according to the specific f_p and *AFD* values of the evaluated case.

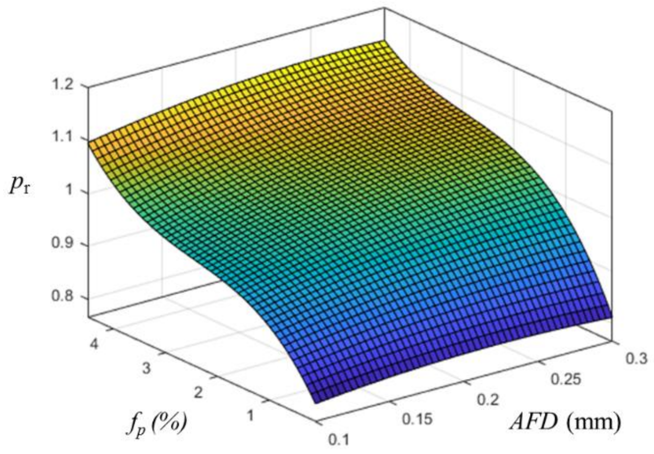

Fig. 7. $p_r(f_p,AFD)$ response surface.

$$p_r(f_p, AFD) = p_{00} + p_{10}AFD + p_{01}f_p + p_{20}AFD^2 + p_{11}AFD \cdot f_p + p_{02}f_p^{\,2} + p_{21}AFD^2 \cdot f_p + p_{12}AFD \cdot f^2 + p_{03}f^3 \quad (11)$$

Where:

p_{00}= 0.7438	p_{10}= 0.5253	p_{01}= 0.1436
p_{20}= -1.259	p_{11}= -0.3574	p_{02}= -0.05718
p_{21}= -0.06387	p_{12}= -0.06466	p_{03}= 0.008743

Once equation (11) was obtained the correction function $C(N_b)$ (12) was determined by applying best fit technique to equation (4) results.

$$C(N_b) = -3.29 \cdot 10^{-7} \cdot N_b + 0.8357 \quad (12)$$

Finally, the propagation model for LPDC A356-T6 alloy (13) was assembled based on equations (2), (11) and (12)

$$N_p(f_p, AFD) = \left(\frac{S_a}{\sigma'_f}\right)^{\frac{1}{b}} \frac{-3.29 \cdot 10^{-7} \cdot N_b + 0.8357}{p_{00} + p_{10}AFD + p_{01}f_p + p_{20}AFD^2 + p_{11}AFD \cdot f_p + p_{02}f_p^{\,2} + p_{21}AFD^2 \cdot f_p + p_{12}AFD \cdot f^2 + p_{03}f^3} \quad (13)$$

Where:

p_{00}= 0.7438	p_{10}= 0.5253	p_{01}= 0.1436
p_{20}= -1.259	p_{11}= -0.3574	p_{02}= -0.05718
p_{21}= -0.06387	p_{12}= -0.06466	p_{03}= 0.008743

4.3 Initiation model

4.3.1 Two-level stress intensity factor sensitivity analysis

Fig. 8 represents the effect on K_{max} of the studied initial pore characteristics. It is observed that in accordance with the literature review [15,24], the more influencing features are d_V, φ and the interaction between them. However, in contrast with Tijani et al. [25] remarks and in accordance with other authors [15,27,28], the morphology of the pores did not have a remarkable influence within the studied range. Based on these results, a second detailed sensitivity study was carried out in order to obtain the $K_{max}(d_v, \varphi)$ surface response.

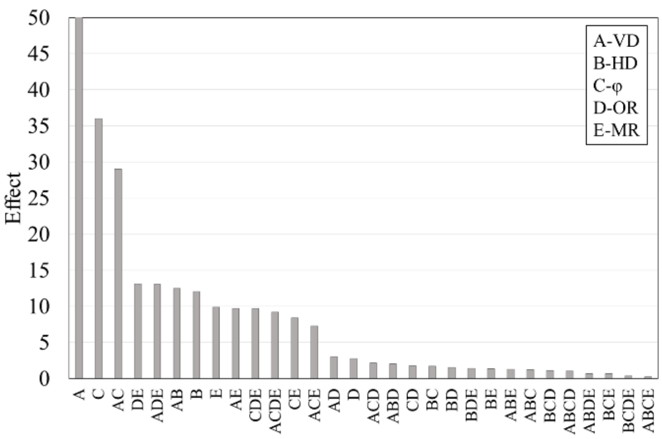

Fig. 8. Results of the two-level sensitivity study

4.3.2 Stress intensity factor response surface

$K_{max}(\varphi, d_V)$ response surface equation (14) was obtained from the detailed sensitivity study which is graphically represented in Fig. 9. Thus, the stress intensity factor based on the initial pore size and distance to the surface of the evaluated case can be estimated within the specified range. It is observed that the pore size becomes especially relevant when the distance to the surface of the pore is short. For higher distances to surface, the pore size does not especially affect in the K_{max} value.

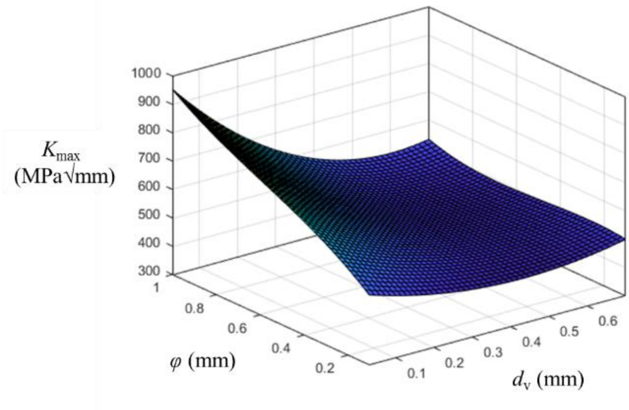

Fig. 9. $K_{max}(\varphi, d_V)$ *response surface*

$$K_{\max}(d_v,\varphi) = k_{00} + k_{10}d_v + k_{01}\varphi + k_{20}{d_v}^2 + k_{11}d_v\cdot\varphi + k_{02}\varphi^2 + k_{21}{d_v}^2\cdot\varphi + k_{12}d_v\cdot\varphi^2 + k_{03}\varphi^3 \quad (14)$$

Where:

k_{00}= 506.4	k_{10}= -216.9	k_{01}= 664.7
k_{20}= 217.6	k_{11}= -1442	k_{02}= -459.1
k_{21}= 1158	k_{12}= 17.84	k_{03}= 308.4

4.3.3 Initiation cycles to total ratio function

Fig. 10 shows the initiation cycles to total ratio function $\alpha(K_{max},N_b)$ (15) for LPDC A356-T6 aluminium alloy, assembled following the methodology explained in section 2.2.2. It is observed that the initiation phase, related to α values, is more relevant in the higher domain of the HCF regime. In addition, for a specific domain inside the HCF regime, the increase of K_{max} values decreases the α values and, consequently, the number of cycles required for crack initiation, which is in agreement with literature [9]. For high K_{max} values, which are related to big pore sizes φ and low distances to surface d_v (see Fig. 9), α values tend to zero, which means that the crack initiation cycles are negligible.

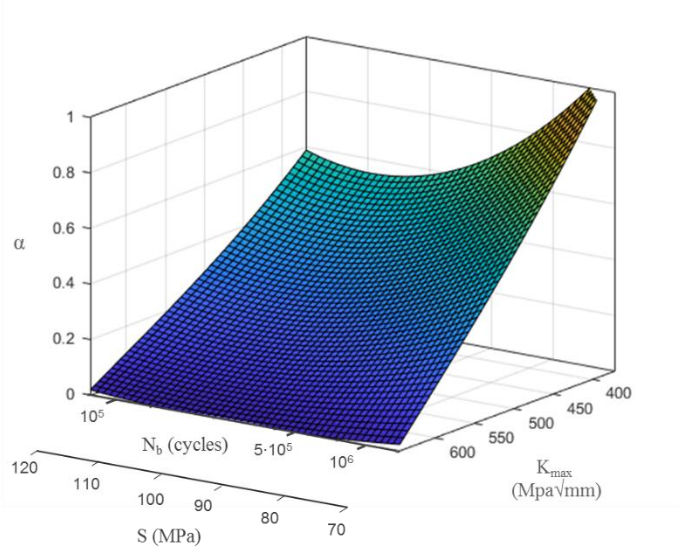

Fig. 10. Surface that relates α, K_{max} and N_b.

$$\alpha(K_{max}, N_b) = a_{n\_00} + a_{n\_10}K_{max} + a_{n\_01}N_b + a_{n\_20}K_{max}^{\ 2} + a_{n\_11}K_{max} \cdot N_b + a_{n\_02}N_b^{\ 2} + a_{n\_21}K_{max}^{\ 2} \cdot N_b + a_{n\_12}N_b \cdot K_{max}^{\ 2} + a_{n\_03}N_b^{\ 3} \tag{15}$$

Where:

a_{n_00}= 1.467	a_{n_10}= 8.107·10^{-7}	a_{n_01}= -0.002779
a_{n_20}= 7.371·10^{-14}	a_{n_11}= -1.689·10^{-9}	a_{n_02}= 5.495·10^{-7}
a_{n_21}= -1.372·10^{-16}	a_{n_12}= 7.033·10^{-13}	a_{n_03}= 3.808·10^{-10}

However, in order to estimate the fatigue life for a certain load stress amplitude, equation (15) was rewritten as $\alpha(K_{max},S_a)$ (16), dependent on S_a, by combining with Basquin (1).

$$\alpha(K_{max}, S_a) = a_{s\_00} + a_{s\_10}K_{max} + a_{s\_01}S_a + a_{s\_20}K_{max}^{\ 2} + a_{s\_11}K_{max} \cdot S_a + a_{s\_02}S_a^{\ 2} + a_{s\_21}K_{max}^{\ 2} \cdot S_a + a_{s\_12}S_a \cdot K_{max}^{\ 2} + a_{s\_03}S_a^{\ 3} \tag{16}$$

Where:

a_{s_00}= 14.07	a_{s_10}= -0.1966	a_{s_01}= -0.02992
a_{s_20}= 8.569·10^{-4}	a_{s_11}= 3.151·10^{-4}	a_{s_02}= 1.917·10^{-5}
a_{s_21}= -1.267·10^{-6}	a_{s_12}= -3.448·10^{-8}	a_{s_03}= -8.848·10^{-9}

4.4 *Porosity based life prediction model for LPDC A356-T6*

Finally, the porosity based life prediction analytic model for LPDC A356-T6 aluminium alloy (17) was obtained considering $N_p(f_p, AFD)$ equation (13), and $\alpha(K_{max},S_a)$ function (16).

$$N_t = \frac{\left(\frac{S_a}{\sigma'_f}\right)^{\frac{1}{b}} \frac{-3.29\cdot 10^{-7}\cdot N_b + 0.8357}{p_{00}+p_{10}AFD+p_{01}f_p+p_{20}AFD^2+p_{11}AFD\cdot f_p+p_{02}f_p^2+p_{21}AFD^2\cdot f_p+p_{12}AFD\cdot f^2+p_{03}f^3}}{1-(a_{s\_00}+a_{s\_10}K_{max}+a_{s\_01}S_a+a_{s\_20}K_{max}^2+a_{s\_11}K_{max}\cdot S_a+a_{s\_02}S_a^2+a_{s\_21}K_{max}^2\cdot S_a++a_{s\_12}S_a\cdot K_{max}^2+a_{s\_03}S_a^3)} \quad (17)$$

Where:

p_{00}= 0.7438	p_{10}= 0.5253	p_{01}= 0.1436
p_{20}= -1.259	p_{11}= -0.3574	p_{02}= -0.05718
p_{21}= -0.06387	p_{12}= -0.06466	p_{03}= 0.008743
a_{00}= 14.07	a_{10}= -0.1966	a_{01}= -0.02992
a_{20}= $8.569\cdot10^{-4}$	a_{11}= $3.151\cdot10^{-4}$	a_{02}= $1.917\cdot10^{-5}$
a_{21}= $-1.267\cdot10^{-6}$	a_{12}= $-3.448\cdot10^{-8}$	a_{03}= $-8.848\cdot10^{-9}$

4.5 *Validation*

The porosity based life prediction model for LPDC A356-T6 was validated with additional fatigue tests at 110, 100, 85 and 75 MPa stress amplitude loads (Fig. 11).

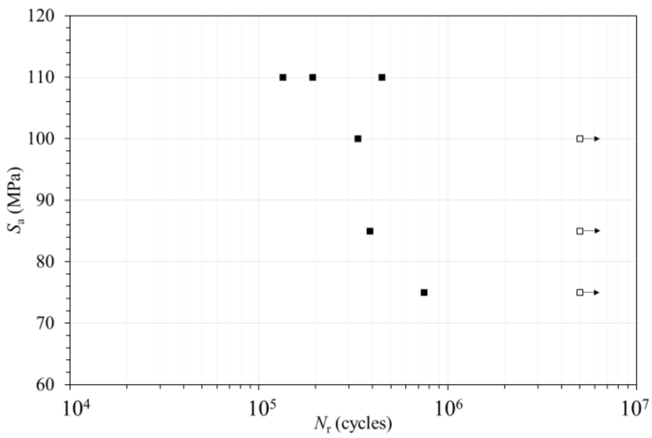

Fig. 11. S-N curve for validation tests.

4.5.1 *Fractographic analysis*

Table 5 shows each validation test life as well as the f_p, *AFD*, φ and d_v parameters measured during the fractographic analysis. In the case of Run Out tests, those parameters could not be measured as the rupture of the specimens did not occur.

Table 5. f_p, *AFD*, φ, d_v *values for validation samples.*

Id.	S_a **(MPa)**	N_{exp} **cycles**	**Fractographic porosity**		**Initial pore**	
			f_p **(%)**	***AFD*** **(mm)**	φ **(mm)**	d_V **(mm)**
V_110_1	110	446564	0.76	0.13	0.058	0.065
V_110_2	110	192410	0.83	0.12	0.414	0.044
V_110_3	110	133879	2.08	0.4	0.312	0
V_100_1	100	334254	0.48	0.12	0.146	0
V_100_2	100	RO	-	-	-	-
V_85_1	85	387002	0.99	0.11	0.529	0
V_85_2	85	RO	-	-	-	-
V_75_1	75	748150	0.72	0.1	205	0.046
V_75_2	75	RO	-	-	-	-

4.5.2 *Model validation*

The validation of the model was performed in two stages. Firstly, the validity of the model to estimate the fatigue life of the specimens used in the S-N curve characterisation was evaluated (Table 6). Secondly, the validity of the model to estimate the fatigue life of additional fatigue tests, which data was not used to build the model, was evaluated (Table 7).

Fig. 12. represents experimental life (solid colour) of both characterisation (circles) and validation samples (squares), together with life estimations obtained with the porosity model for each case (empty circles and squares respectively). It is remarkable that for each tested load amplitude, the proposed model predicts, in all cases, which are the specimens that present higher and lower life, while conventional fatigue models provide a single life prediction for each tested load case.

Table 6. Experimental life vs. theoretical life of the S-N characterisation specimens.

Id.	S_a (MPa)	N_{exp} (cycles)	N_b (cycles)	N_p (cycles)	K_{max} (MPa √mm)	α	N_t (cycles)	*Log error (%)*	*Abs error (%)*
C_120_1	120	155765	107871	97917	474	0.34	146334	0.52	6.1
C_120_2	120	145470	107871	91218	615	0.08	96823	3.42	33.4
C_120_3	120	81898	107871	83195	761	0	82135	0.03	0.3
C_110_1	110	189654	167364	145754	547	0.17	172604	0.78	9.0
C_110_2	110	164285	167364	116224	777	0	116163	2.89	29.3
C_110_3	110	236106	167364	148960	420	0.41	251239	0.50	6.4
C_90_1	90	344584	460884	346327	661	0	340539	0.09	1.2
C_90_2	90	352414	460884	312606	649	0	308609	1.04	12.4
C_90_3	90	437269	460884	355067	454	0.43	613497	2.61	40.3
C_80_1	80	599318	835232	892415	525	0.35	766008	1.84	27.8
C_80_2	80	1393739	835232	911283	428	0.65	1472485	0.39	5.6
C_80_3	80	495164	835232	905075	555	0.27	686506	2.49	38.6
C_70_1	70	1550358	1638883	1695154	514	0.53	1018211	2.95	34.3
C_70_2	70	447473	1638883	1471001	428	0	449074	0.03	0.4
C_70_3	70	Run Out	1638883	-	-		146334	-	-

Table 7. Experimental life vs. theoretical life of validation specimens.

Id.	S_a (MPa)	N_{exp} (cycles)	N_b (cycles)	N_p (cycles)	K_{max} (MPa √mm)	α	N_t (cycles)	*Log error (%)*	*Abs error (%)*
V_110_1	110	446564	167364	182006	343	0.63	390259	1.04	12.6
V_110_2	110	192410	167364	145061	619	0.05	151328	1.97	21.4
V_110_3	110	133879	167364	142841	592.9	0.09	135747	0.12	1.4
V_100_1	100	334254	270776	283856	474	0.31	331990	0.05	0.7
V_100_2	100	RO	-	-	-	-	-	-	-
V_85_1	85	387002	615035	664276	748	0	426426	0.75	10.2
V_85_2	85	RO	-	-	-	-	-	-	-
V_75_1	75	748150	1156898	579391	371	0.5	944406	1.72	26.2
V_75_2	75	RO	-	-	-	-	-	-	-

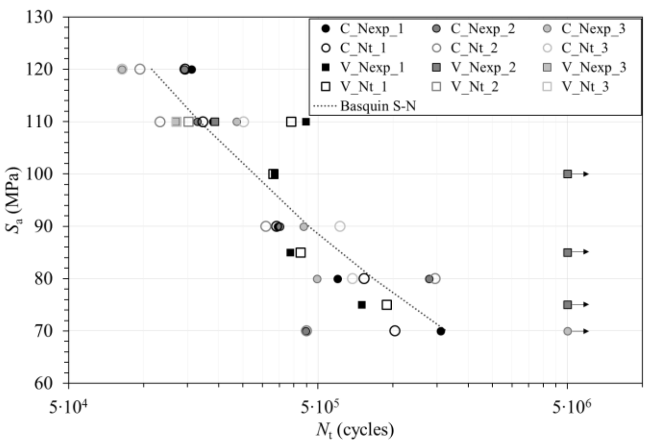

Fig. 12. Life predictions using the proposed model.

Fig. 13 presents the life prediction logarithmic error of both the proposed model and Basquin model. It is observed that the quantitative life prediction of the proposed model presents in most cases a logarithmic error below 2 % and an absolute error below 16%. However, in some cases the quantitative life prediction presents logarithmic errors up to 3 % (40% absolute error) which indicates that even the porosity is the main affecting parameter, there are other affecting variables not considered in the model. Fig. 14 shows an example of the fractographic surfaces of samples C_110_1 and C_80_3. In the first, a high amount of inclusions was found while in the second, a big pore near the initiation pore that could accelerate initiation was observed.

Nevertheless, the maximum logarithmic error in life prediction of 3.4% (33.4% absolute error) obtained with the proposed model is still below the maximum logarithmic error of 10% (266% absolute error) that Basquin model presents.

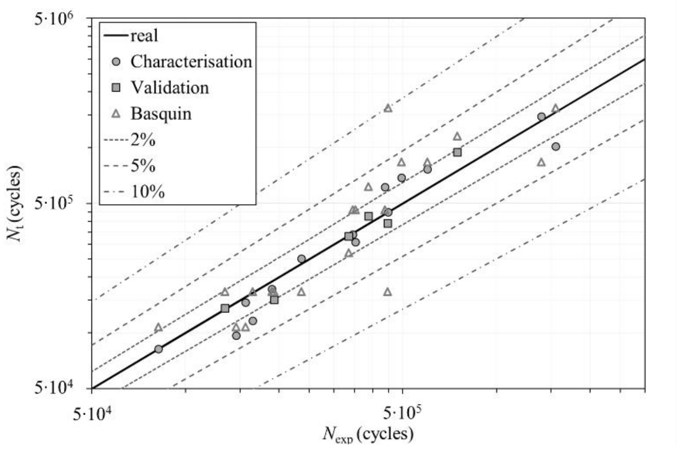

Fig. 13. Comparison of predicted to real cycle error of the proposed porosity model and Basquin model.

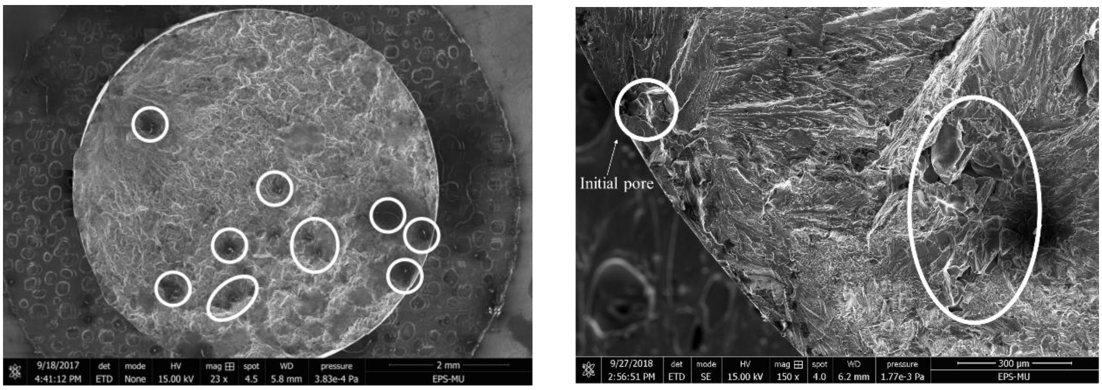

(a) (b)

Fig. 14. Detailed fracture surfaces in specimens a) C_100_1 and b) C_80_3

5 CONCLUSIONS

Nowadays, most of fatigue assessment models are not able to consider the scatter of different samples tested at the same load. Although there are many sources that generate this variability in the fatigue behaviour, porosity is one of the main affecting parameters in the fatigue scatter of casting components. Therefore, in the present work an alternative fatigue assessment procedure, which accounts the effect of porosity on the initiation and propagation phases, was developed and implemented for LPDC A356-T6 aluminium alloy.

Results have shown that considering the effect of porosity in both initiation and propagation phases, it is possible to predict qualitatively the scatter trend of each tested sample in all tested cases. Moreover, quantitative life prediction presents an average logarithmic error below 2% and an absolute average error below 16% in life prediction. However, porosity is not the only affecting parameter in fatigue life scatter. Thus, quantitative logarithmic deviations up to 3.4 % and absolute deviations up to 40 % were found in some cases. Fractographic analysis showed that, for example, higher or lower inclusion level that the average of the specimens tested to build the model or the existence of big pores in the subsurface near the initiation pore can directly affect in the fatigue life prediction.

The main drawback of the presented fatigue assessment model is that the required porosity parameters, f_p, *AFD*, φ and d_v, are difficult to measure before the rupture of the tested sample. Thus, in order to use the proposed procedure as a predictive tool in the design process of casting parts, it is necessary an extended statistic data base of the typical f_p, *AFD*, φ and d_v values of tested components that represent the process window. Therefore, the proposed model is appropriate for autopart manufacturing industry were high series of different components in same material are produced. Thus, once the process window is characterised, the acceptance limits of f_p, *AFD*, φ and d_v can be defined. This limit values can be implemented in the proposed model during the design process ensuring the fatigue performance of accepted components.

Acknowledgments

The authors would like to thank FAGOR Ederlan Group for the support in the development of the present work. In addition, authors would like to acknowledge the financial support provided by the Ministry of Industry Economics and Competitiveness of the Spanish Government by means of ALPRE project (RTC-2015-3822-4) and the FEDER funds from the European Union.

References

[1] Stephens R., Fatemi A, Stephens RR, Fuchs H. Metal fatigue in engineering 2001.

[2] Yi JZ, Gao YX, Lee PD, Flower HM, Lindley TC. Scatter in fatigue life due to effects of porosity in cast A356-T6 aluminum-silicon alloys. Metall Mater Trans A 2003;34:1879–90. doi:10.1007/s11661-003-0153-6.

[3] Bonollo F, Urban J, Bonatto B, Botter M. Gravity and low pressure die casting of aluminium alloys: a technical and economical benchmark. La Metall Ital 2005:23–32.

[4] Iben Houria M, Nadot Y, Fathallah R, Roy M, Maijer DM. Influence of casting defect and SDAS on the multiaxial fatigue behaviour of A356-T6 alloy including mean stress effect. Int J Fatigue 2015;80:90–102. doi:10.1016/j.ijfatigue.2015.05.012.

[5] Roy MJ, Nadot Y, Nadot-Martin C, Bardin PG, Maijer DM. Multiaxial Kitagawa analysis of A356-T6. Int J Fatigue 2011;33:823–32. doi:10.1016/j.ijfatigue.2010.12.011.

[6] Wang QG, Apelian D, Lados D a. Fatigue behavior of A356-T6 aluminum cast alloys. Part I. Effect of casting defects. J Light Met 2001;1:73–84. doi:10.1016/S1471-5317(00)00008-0.

[7] Lee C Do, Yoo SJ. Dependence of Fatigue Life of Low-Pressure Die-Cast A356 Aluminum Alloy on Microporosity Variation. Met Mater Int 2014;20:601–12. doi:10.1007/s12540-014-4004-3.

[8] Zheng X, Cui H, Engler-Pinto CC, Su X, Wen W. Statistical relationship between fatigue crack initiator size and fatigue life for a cast aluminum alloy. Mater Sci Eng A

2013;580:71–6. doi:10.1016/j.msea.2013.05.045.

[9] Ammar HR, Samuel AM, Samuel FH. Porosity and the fatigue behavior of hypoeutectic and hypereutectic aluminum–silicon casting alloys. Int J Fatigue 2008;30:1024–35. doi:10.1016/j.ijfatigue.2007.08.012.

[10] Avalle M, Belingardi G, Cavatorta MP, Doglione R. Casting defects and fatigue strength of a die cast aluminium alloy: A comparison between standard specimens and production components. Int J Fatigue 2002;24:1–9. doi:10.1016/S0142-1123(01)00112-8.

[11] Ammar HR, Samuel AM, Samuel FH. Effect of casting imperfections on the fatigue life of 319-F and A356-T6 Al–Si casting alloys. Mater Sci Eng A 2008. doi:10.1016/j.msea.2007.03.112.

[12] González R, González A, Talamantes-Silva J, Valtierra S, Mercado-Solís RD, Garza-Montes-De-Oca NF, et al. Fatigue of an aluminium cast alloy used in the manufacture of automotive engine blocks. Int J Fatigue 2013;54:118–26. doi:10.1016/j.ijfatigue.2013.03.018.

[13] Li B, Shen Y, Hu W. Casting defects induced fatigue damage in aircraft frames of ZL205A aluminum alloy - A failure analysis. Mater Des 2011;32:2570–82. doi:10.1016/j.matdes.2011.01.039.

[14] Le V-D, Morel F, Bellett D, Pessard E, Saintier N, Osmond P. Microstructural-based Analysis and Modelling of the Fatigue Behaviour of Cast Al-Si Alloys. Procedia Eng 2015;133:562–75. doi:10.1016/j.proeng.2015.12.630.

[15] Murakami Y. Material defects as the basis of fatigue design. Int J Fatigue 2012;41:2–10. doi:10.1016/j.ijfatigue.2011.12.001.

[16] Susmel L, Taylor D. On the use of the Theory of Critical Distances to predict static failures in ductile metallic materials containing different geometrical features. Eng Fract Mech 2008;75:4410–21. doi:10.1016/j.engfracmech.2008.04.018.

[17] Nadot Y, Billaudeau T. Multiaxial fatigue limit criterion for defective materials. Eng Fract

Mech 2006;73:112–33. doi:10.1016/j.engfracmech.2005.06.005.

[18] Tenkamp J, Koch A, Knorre S, Krupp U, Michels W, Walther F. Defect-correlated fatigue assessment of A356-T6 aluminum cast alloy using computed tomography based Kitagawa-Takahashi diagrams. Int J Fatigue 2018;108:25–34. doi:10.1016/j.ijfatigue.2017.11.003.

[19] Linder J, Axelsson M, Nilsson H. The influence of porosity on the fatigue life for sand and permanent mould cast aluminium. Int J Fatigue 2006;28:1752–8. doi:10.1016/j.ijfatigue.2006.01.001.

[20] Leitner M, Garb C, Remes H, Stoschka M. Microporosity and statistical size effect on the fatigue strength of cast aluminium alloys EN AC-45500 and 46200. Mater Sci Eng A 2017;707:567–75. doi:10.1016/j.msea.2017.09.023.

[21] Ammar HR, Samuel AM, Samuel FH. Effect of casting imperfections on the fatigue life of 319-F and A356-T6 Al–Si casting alloys. Mater Sci Eng A 2008;473:65–75. doi:10.1016/j.msea.2007.03.112.

[22] Spangenberger AG, Lados DA, Coleman M, Birosca S, Hardy MC. Microstructural mechanisms and advanced characterization of long and small fatigue crack growth in cast A356-T61 aluminum alloys. Int J Fatigue 2017;97:202–13. doi:10.1016/j.ijfatigue.2016.12.029.

[23] Llavori I. Simulación numérica y validación experimental de fenómenos de desgaste y fatiga por fretting en aceros trefi lados de reducido diámetro. 2016.

[24] Ueno A, Miyakawa S, Yamada K, Sugiyama T. Fatigue behavior of die casting aluminum alloys in air and vacuum. Procedia Eng 2010;2:1937–43. doi:10.1016/j.proeng.2010.03.208.

[25] Tijani Y, Heinrietz A, Bruder T, Hanselka H. Quantitative evaluation of fatigue life of cast aluminum alloys by non-destructive testing and parameter model. Int J Fatigue 2013;57:73–8. doi:10.1016/j.ijfatigue.2013.05.017.

[26] https://imagej.nih.gov/ij/ n.d.

[27] Rotella A, Nadot Y, Piellard M, Augustin R, Fleuriot M. Fatigue limit of a cast Al-Si-Mg alloy (A357-T6) with natural casting shrinkages using ASTM standard X-ray inspection. Int J Fatigue 2018;114:177–88. doi:10.1016/j.ijfatigue.2018.05.026.

[28] Wang QG, Davidson CJ, Griffiths JR, Crepeau PN. Oxide Films, Pores and the Fatigue Lives of Cast Aluminum Alloys. Metall Mater Trans B 2006;37B:889–95.